Materials Research Proceedings 28 (2023) 657-666 https://doi.org/10.21741/9781644902479-71

An analytical approach for modelling incremental disk rolling process

ACAR Sadik Sefa [1,3,a *], DINÇER Mehmet Şamil [2,3,b] and OZCATALBAS Mustafa[3,c]

[1]Department of Aerospace Engineering, Middle East Technical University, Ankara, Turkey

[2]Department of Metallurgical and Materials Engineering, Middle East Technical University, Ankara, Turkey

[3]Repkon Machine and Tool Industry and Trade Inc., Istanbul, Turkey

[a]sadik.acar@metu.edu.tr, [b]samil.dincer@metu.edu.tr, [c]mustafa.ozcatalbas@repkon.com.tr

Keywords: Incremental Forming, Disk Rolling, Velocity Field, Strain Rate Field, Analytical Model, Contact Zone, Deformation Field

Abstract. In the context of the current study, an analytical method is developed to determine the deformation field of the workpiece under the forming roller for an unconventional incremental radial disk rolling (IRDR) process. As the industrial forming machine is in the development phase, the machine and process design requires a preliminary assessment tool that is sensitive to process parameters and roller geometry. Establishing a parametric relationship between process parameters and induced deformation field enables designers to determine the parameters needed to obtain the target geometry and microstructure as well as the forming machine requirements. Instantaneous roller-workpiece interface, i.e. contact zone, and cross-sections that plastic flow occurs in between are calculated. The contact zone is spatially discretized to two-dimensional surface elements. The principle of volume conservation during plastic deformation is utilized to obtain velocity fields in three dimensions. Strain rate distributions are calculated by taking the gradient of the velocity fields in respective directions. Average values of strain at each cross-section are the accumulated plastic strain that is created by the multiple circumferential passes of the roller and computed numerically, accounting for different strain rates and contact times at each pass. Obtained contact zone geometries, deformation fields, and the effect of different process parameters are discussed. Results show that deformation occurs mainly in the circumferential direction and the tangential velocity of the roller in the circumferential direction has a more pronounced effect on the deformation than the radial advance of the roller per revolution.

Introduction

Having a firm grip on the deformation of the material is essential in a forming operation. Controlling the deformation allows for avoiding possible failures, defects, and undesired inhomogeneities and estimating other crucial forming phenomena such as residual stresses, springback, buckling, pile-up at the onset of forming zone, and diametral growth for cylindrical and disk-shaped products [1,2]. Also, the deformation has a significant effect on the microstructural evolution during the process which affects the mechanical performance of the final product [3]. Microstructural effects are important especially for the hot forming operations due to the recrystallization and grain growth which are usually dictated by narrow temperature, deformation, and time limitations [4]. Therefore, obtaining the desired microstructure depends on the degree of control the process designer can exert on the deformation of the material.

In the literature, mathematical models are often used to assess the deformation of the material in forming operations [5]. One of these methods is the upper-bound method which utilizes an energy functional that has to be minimized to obtain the correct kinematically admissible velocity

field. Kinematic admissibility was derived from the incompressible volume principle [6]. Rolling applications combined the analytical methods with the finite element method for plane-strain rolling [7]. Analytical methods are used to provide the material property update to the finite element model [8]. The volumetric restrictions and plastic flow velocity field are often determined by different approaches based on the upper-bound method such as arc tangent velocity field and cosine velocity field methods [9,10]. The analytical methods are employed to optimize the process parameters of wire flat rolling [11]. The aim was mainly the determination of required rolling force and torque [12]. In extrusion problems, velocity fields had to be substantially modified according to the die geometry [13].

The incremental radial disk rolling (IRDR) process employs two forming rollers which are positioned reciprocally and pulled radially outward. Rollers form the rotating workpiece disk to a higher diameter and a lower thickness. One of the differences between conventional rolling processes and IRDR process is that the axis of roller rotation is either parallel to the axis of the roller feed (radial) or located on the radial-axial(thickness) plane for IRDR while the axis of roller rotation and axis of roller feed are generally perpendicular to each other in conventional rolling [14]. Another difference is that a relatively smaller portion of the workpiece material is subjected to plastic deformation at any instant during the IRDR process. Compared to conventional rolling processes, tube spinning is more similar to IRDR. Apart from the final workpiece shape, the difference distinguishing IRDR from tube spinning is that circumference of the roller path increases and the curvature of the material under the contact zone decreases as the roller moves away from the centre of the disk throughout the IRDR process. Therefore, ensuring the plastic flow stability and homogenous deformation during the IRDR process is much more difficult [15].

Previous studies investigated relatively simpler deformation states of conventional rolling processes. Developed models considered much simpler tool designs and contact zones as the current process requires a complex tool geometry. Also, deformation fields for the current rolling machine have never been researched before. This study focuses on developing parametrical velocity field, strain, and strain rate expressions accounting for any tool geometry, workpiece geometry, and process parameter set. The study aims to provide a preliminary assessment tool for the optimization of the process and the roller geometry for the IRDR process. An analytical method is developed and utilized to determine strain and strain rate distribution in the workpiece material under the forming roller. The forming machine is still in the development phase and optimization of the process requires the evaluation of an extensive number of combinations of process and roller parameters. Even though approaches involving the finite element method are useful, their computational cost is extremely high compared to the current method. Therefore, far fewer finite element method (FEM) simulations are needed in cooperation with the current method. A validation study of the current method with experiments and FEM is in progress. Also in future works, the deformation fields found by the current method will be employed to determine roller geometry and process parameter ranges satisfying the requirements derived from time, force, microstructure, and processing map limitations.

Theory

Roller geometry depends on four independent parameters: roller nose radius (R_n), roller radius (R_r), roller attack angle (α), and roller height (Δt) which is equal to the thickness reduction in this study. Roller geometry also includes smooth angle, smooth nose radius, length of the upper levelling, upper levelling draft angle and length of the lower levelling but they are not included in the calculations due to the limitations of the analytical method. Previous studies showed that the length of the upper levelling and the upper levelling draft angle parameters affect the material pile-up at the onset of feed direction and other parameters control mainly the springback and final surface quality [16]. These subjects are not in the context of the current study and can be neglected in the calculations. The general layout of the moving parts of the machine and the roller geometry

is shown in Fig. 1. Workpiece is attached to the mill which provides the rotational drive to the workpiece.

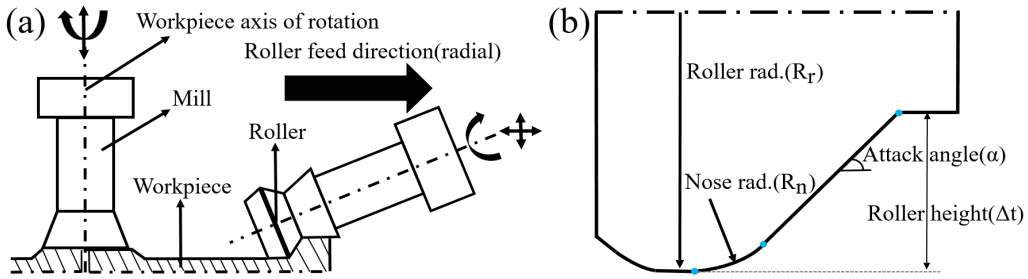

Fig. 1. (a)Layout and motion of roller, mill and workpiece, (b) roller geometry.

The roller is pulled radially outward as the workpiece turns and the roller idles around its axis of rotation. The roller bites the material and the contact zone develops. The area and shape of the contact zone depend on roller geometry, radial feed (f) and radial feed per revolution (pitch, p). Thickness reduction is assumed to be equal to roller height (Δt) to reduce the number of independent variables. The width of the contact zone is assumed to be parallel to the circumferential direction and the system is defined in the Cartesian coordinate system since the width of the contact zone is usually very short compared to the circumference of a near-circular roller path. The origin is defined at a location radially inward by pitch amount with respect to the bottom of the roller nose. The trials with CAD models showed that the contact zone can be represented by a region within seven points, four of which lie on the radial-axial(thickness) plane that the width(b) is zero. Eqs. 1 and 2 provide parametric expressions for radial and axial(thickness) distances between points.

$$L_1 = R_n \sin\alpha, \qquad L_2 = \frac{\Delta t - R_n(1 - \cos\alpha)}{\tan\alpha}, \qquad t_1 = R_n(1 - \cos\alpha), \qquad t_2 = \Delta t - R_n(1 - \cos\alpha) \tag{1}$$

$$t^* = R_r - R_n(1 - \cos\alpha) - \sqrt{\left(R_r - R_n(1 - \cos\alpha)\right)^2 - b_{mid}^2} \tag{2}$$

Broadwise locations of points P_5, P_6 and P_7 are expressed as b_{up}, b_{mid} and b_{low}, respectively. Fig. 2 illustrates point locations which are calculated with found distances. The three-dimensional geometry of the contact zone is obtained parametrically by utilizing cubic area interpolation between these points.

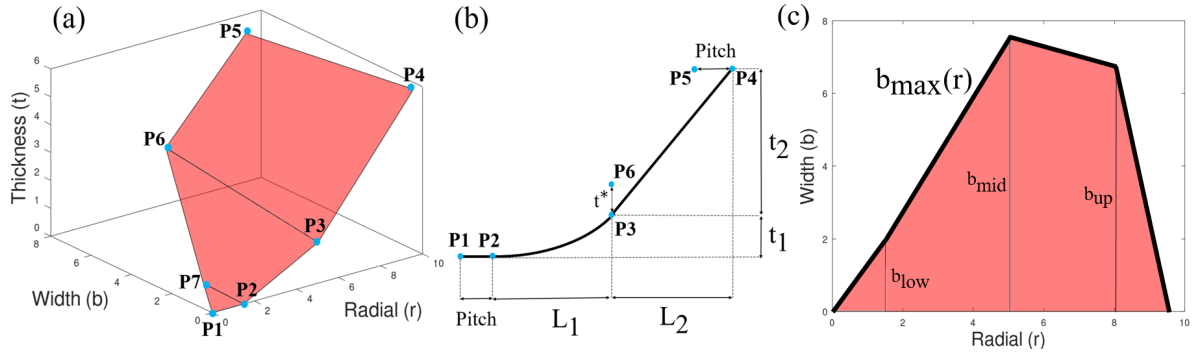

Fig. 2. (a)Points defining the contact zone, (b)Positions of points in radial(r)-axial(t) plane, (c)Maximum width as a function of radial location.

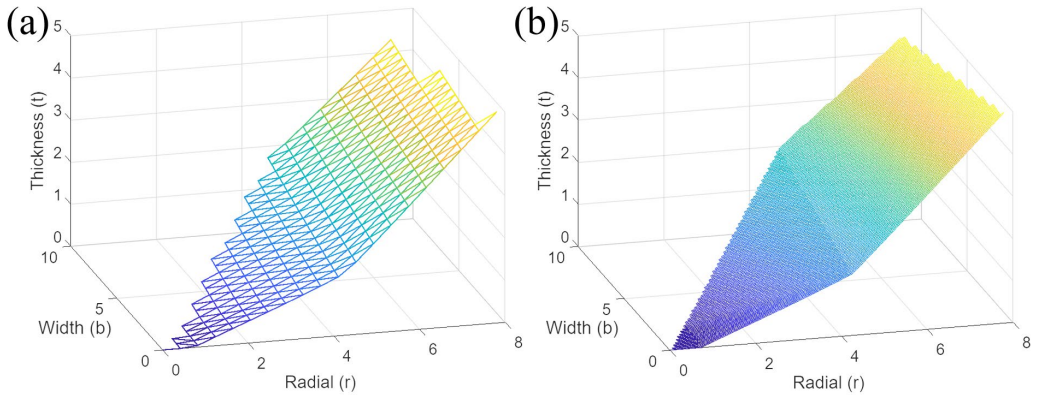

Fig. 3. Discretization of the contact zone with (a)450 and (b)13000 elements.

Interpolated area is spatially discretized into triangular surface elements using Delaunay Triangulation [17]. The centroidal location of each element is calculated and the developed analytical model is implemented on these centroids. Fig. 3 compares contact zones obtained by different mesh densities. The contact zone employing finer mesh which has 13000 surface elements, accurately captured the curvature of the nose region as well as the flatness of the lower levelling region below the nose. Also, the model with finer mesh achieved a more precise contact zone boundary representation.

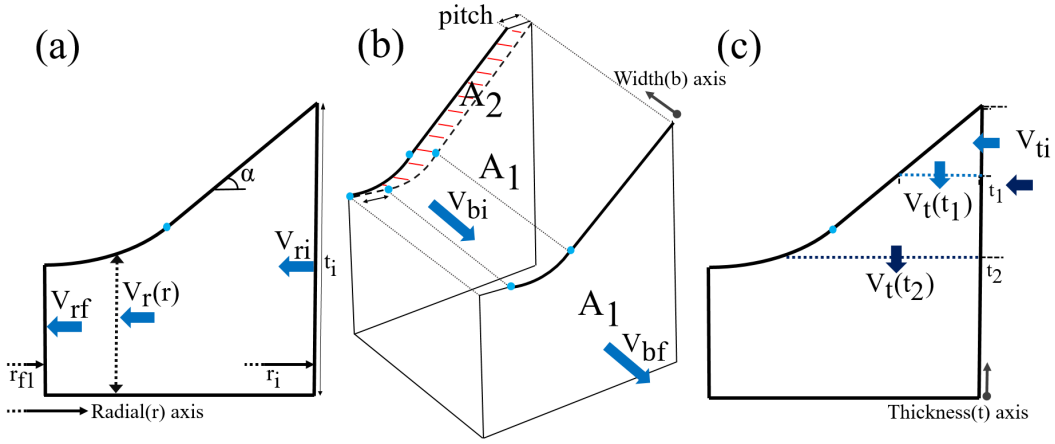

Fig. 4. Plastic flow directions and cross-sections in (a)radial, (b)width and (c)thickness axes.

Derivation of Velocity Field.

The material is assumed to undergo no elastic strain relaxation between circumferential passes since the induced plastic strain is expected to be much higher than the elastic strain. Strain rate calculations start with the derivation of analytic expressions for plastic flow velocities in three axes. Fig. 4 illustrates flow velocities and cross-sections that the flow travels in corresponding directions. Calculations rely on the assumption that plastic deformation induces no volume change. Flow in each direction is assumed to be independent of each other. The tangential velocity of the roller in the circumferential direction is much higher than that in the radial direction for process parameters tested in this study. Therefore the contribution of plastic flow in different directions to each other is negligible. This assumption should be improved in the future. Firstly, initial volumetric flow rates are calculated. Then, cross-sections normal to the flow are parametrically expressed for any location. The plastic velocity that the material has to have while travelling through a defined cross-section is obtained by employing the volume conservation principle. The velocity found is the average velocity of the material flowing below the corresponding point of the roller as the cross-section is dictated by the contact zone and the radial location of the roller, in

Materials Research Proceedings 28 (2023) 657-666 https://doi.org/10.21741/9781644902479-71

addition to process parameters. Finally, strain rate expressions are obtained by taking the gradient of the velocity field along the corresponding direction.

The radial plastic velocity field is illustrated in Fig. 4(a). For calculations, the radial axis is separated into two regions, the inclined region and nose region, divided by the upper end of the roller nose whose radial location (r^*) is formulated in Eq. 3 where r_i is the initial radius. For all calculations, subscript i and the term "initial" denote the initial properties just before entering the contact zone. Radial location of the bottom end of the nose (r_{f1}) is also given in Eq. 3.

$$r^* = r_i - \frac{\Delta t - R_n(1 - \cos\alpha)}{\tan\alpha} \quad \text{and} \quad r_{fl} = r^* - R_n \sin\alpha \tag{3}$$

Only the variation of thickness with radius is different for these two regions. Volume conservation in radial direction and radial flow velocity as a function of radius are expressed in Eq. 4 where feed (f) is the initial radial velocity and t_i is the initial thickness.

$$V_r(r)t(r)\, 2\pi\, r = f\, t_i\, 2\pi\, r_i \;\rightarrow\; V_r(r) = \frac{f\, r_i\, t_i}{r\, t(r)} \tag{4}$$

Variations of thickness with radial location and consequent radial flow velocities are formulated in Eqs. 5 and 6.

$$t(r) = t_i + \frac{r - r_i}{\tan\alpha} \quad \rightarrow \quad V_r(r) = \frac{f\, r_i\, t_i\, \tan\alpha}{r\,(t_i\, \tan\alpha + r - r_i)} \qquad \text{for} \quad r^* < r < r_i \tag{5}$$

$$t(r) = t_f + R_n - \sqrt{R_n^2 - (r - r_{fl})^2} \;\rightarrow\; V_r(r) = \frac{f\, r_i\, t_i}{r\,(t_f + R_n - \sqrt{R_n^2 - (r - r_{fl})^2})} \quad \text{for} \quad r_{fl} < r < r^* \tag{6}$$

Circumferential plastic flow is shown in Fig. 4(b). Material starts to flow under the roller when it encounters the furthest point of the contact zone in the width axis: b_{mid} which is broadwise location of P_6 shown in Fig. 2(a). The initial cross-section that plastic flow velocity passes has an area of A_1+A_2. As the flow continues under the contact zone, the cross-sectional area is assumed to be linearly decreased to A_1. A_2 is the projectional area of the contact zone on the radial-axial plane and equal to pitch times Δt. The expression found for A_1 is given in Eq. 7.

$$A_1 = t_f\,(R_n \sin\alpha + p) + \frac{t_i^2 - (t_f + R_n\,(1 - \cos\alpha))^2}{2\tan\alpha} + R_n^2\,(\sin\alpha\left(1 - \frac{\cos\alpha}{2}\right) - \frac{\alpha(\text{rad})}{2}) \tag{7}$$

Volume conservation in the width axis and resulting relation for circumferential velocity field expression are presented in Eqs. 8 and 9 where V_{bi} is the known initial tangential velocity in the circumferential direction. Variation of the cross-sectional area with broadwise location is obtained by the use of assumed linear area decrease between $b = b_{mid}$ *and* $b = 0$.

$$V_b(b)A(b) = V_{bi}\,(A_1 + A_2) \;\rightarrow\; V_b(b) = V_{bi}\,\frac{(A_1 + A_2)}{A(b)} \tag{8}$$

$$A(b) = A_1 + A_2\,\frac{b}{b_{mid}} \;\rightarrow\; V_b(b) = V_{bi}\, b_{mid}\,\frac{A_1 + A_2}{A_1\, b_{mid} + A_2\, b} \tag{9}$$

In radial and circumferential velocity field calculations, initial cross-sections were assumed to be constant and all cross-sections were parallel to each other. In contrast, for the axial velocity field, the initial cross-section has normal in the radial direction and it is assumed to be a function of thickness. Because, the material enters the contact zone in the radial direction and is pressed downward in the axial axis at any point on the roller, as demonstrated in Fig. 4(c). The expression for axial plastic velocity is formulized in Eq. 10.

$$V_t(t)\,(r_i - r)\,2\pi\,\frac{r_i + r}{2} = f\,(t_i - t)\,2\pi\, r_i \;\rightarrow\; V_t(t) = 2f\, r_i\,\frac{(t_i - t)}{(r_i - r)(r_i + r)} \tag{10}$$

Axial flow velocity as a function of axial location is presented in Eq. 11.

$$r = r_i - (t_i - t)\tan\alpha \;\rightarrow\; V_t(t) = \frac{2f\,r_i}{\tan\alpha\left(2\,r_i - (t_i - t)\tan\alpha\right)} \tag{11}$$

Strain Rate Distribution.

Strain rates are calculated by taking the gradient of the velocity field in respective directions. Eqs. 12 and 13 provide the radial strain rate expression which is the gradient of Eqs. 5 and 6 in the radial direction.

$$\dot{\varepsilon}_r = \frac{dV_r}{dr} = f\,r_i\,t_i\,\tan\alpha\,\frac{-t_i\,\tan\alpha - 2r + r_i}{r^2(t_i\,\tan\alpha + r - r_i)^2} \quad \text{for} \quad r^* < r < r_i \tag{12}$$

$$\dot{\varepsilon}_r = \frac{dV_r}{dr} = f\,r_i\,t_i\,\frac{-\sqrt{R_n^2 - (r - r_{fl})^2}\,(t_f + R_n) + R_n^2 - (r - r_{fl})^2 - r\,(r - r_{fl})}{r^2\sqrt{R_n^2 - (r - r_{fl})^2}\left(t_f + R_n - \sqrt{R_n^2 - (r - r_{fl})^2}\right)^2} \quad \text{for} \quad r_{fl} < r < r^* \tag{13}$$

Circumferential and axial strain rate relations are shown in Eqs. 14 and 15 which are gradients of velocity fields in circumferential (b) and axial (t) directions, see Eqs. 9 and 11, respectively.

$$\dot{\varepsilon}_b = \frac{dV_b}{db} = -V_{bi}\,b_{mid}\,\frac{A_2\,(A_1 + A_2)}{(A_1\,b_{mid} + A_2\,b)^2} \tag{14}$$

$$\dot{\varepsilon}_t = \frac{dV_t}{dt} = -\frac{2f\,r_i}{(2\,r_i - (t_i - t)\tan\alpha)^2} \tag{15}$$

Strain Distribution.

Strain at each element is considered as the cumulative plastic strain induced by circumferential passes of the roller. At each circumferential pass, the material is subjected to varying strain rates under the contact zone in three directions. As the strain rate distributions are found, strain increments ($\Delta\varepsilon_j$) at each pass and the sum of the strain increments (ε_j, accumulated strain) can be calculated according to Eq. 16 for each element. In the strain equation, j is the direction of the strain and strain rate, e is the domain of locations that the element presented at previous passes and Δt(e) is the duration of contact time for each location. b_{max} values are calculated by interpolation between b_{up}, b_{mid} and b_{low} at known previous radial locations as shown in Fig. 2(c).

$$\varepsilon_j = \sum_e \Delta\varepsilon_j\,(e) = \sum_e \Delta t(e)\,\dot{\varepsilon}_j(e) \quad \text{where} \quad \Delta t(e) = \frac{b_{max}(e)}{V_{bi}} \tag{16}$$

Results

The workpiece material and the process temperature does not affect the results of this study. Also, even though the developed method is capable of accounting for varying initial radii, all calculations in this study are done for only one value of initial radius which is 120 mm. It is found that the contact zone changes as the roller moves in the radial axis for low radii. As the roller further moves away from the centre, the contact zones at different radial locations become very similar. The employed initial radius is chosen to be obeying the second trend. Also, a mesh dependency study is carried out but it is not presented here to restrict the extent of the paper. Results for only the finer mesh are evaluated. Firstly, the effect of roller geometry on the contact zone is investigated. Four roller geometry (RG) parameter sets are created and tabulated in Table 1. Obtained contact zones are shown in Fig. 5. To preserve comparability, each contact zone was formed by the same process parameter set which is 0.3 mm/s feed rate(f) and 25 RPM spindle rate. A higher roller radius leads to a wider contact zone, comparing RG1 and RG2. Contact zones of RG1 and RG3

show the effects of nose radius and roller height. The inclined region constitutes a much higher portion of the contact zone than the nose region for the roller with a lower R_n and higher Δt. Also, increased roller height elongated the contact zone in the radial direction. Examining the contact zone of RG4, a low attack angle also causes a significant increase in the radial length of the contact zone.

Table 1. Dimensions of 4 different roller geometries (RG).

	Roller Radius, R_r [mm]	Nose Radius, R_n [mm]	Attack Angle, α [°]	Roller height, Δt [mm]
RG1	35	5	45	5
RG2	70	5	45	5
RG3	35	2.5	45	7.5
RG4	70	2.5	30	7.5

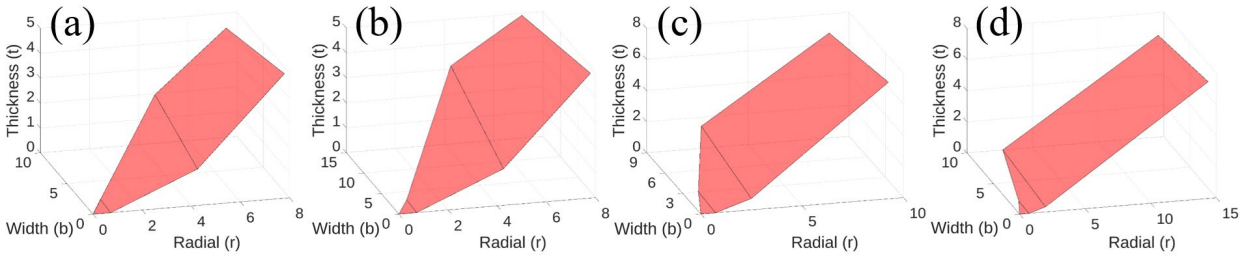

Fig. 5. Contact zones of (a) RG1, (b) RG2, (c) RG3 and (d) RG4 for w=25 RPM, f=0.3 mm/s.

For investigations on deformation distribution, only one roller geometry which is RG1, is employed so that the effect of process parameters could be examined clearly. The effect of roller geometry on the deformation will be studied in the future. Fig. 6 shows directional and the von Mises equivalent strain rate distributions. The radial strain rate ($\dot{\varepsilon}_r$) is equal to zero at the beginning of the radial axis for a pitch amount of length since that region is flat and induces no radial deformation. Then, the magnitude of the $\dot{\varepsilon}_r$ increases with r because the round profile of the nose region leads to higher cross-sectional area differences between different radial locations on the nose region. On the inclined region, the magnitude of $\dot{\varepsilon}_r$ linearly decreases with r due to the increasing thickness of the workpiece.

Circumferential strain rate ($\dot{\varepsilon}_b$) values are similar along the width axis. Magnitude of $\dot{\varepsilon}_b$ is much higher than strain rates in other directions which shows that material flows mainly in the width axis. Axial strain rate ($\dot{\varepsilon}_t$) is very small and almost constant along the contact zone. Along the radial axis on the b=0 plane, the equivalent von Mises strain rate is around 1.3 for the given process and roller parameters.

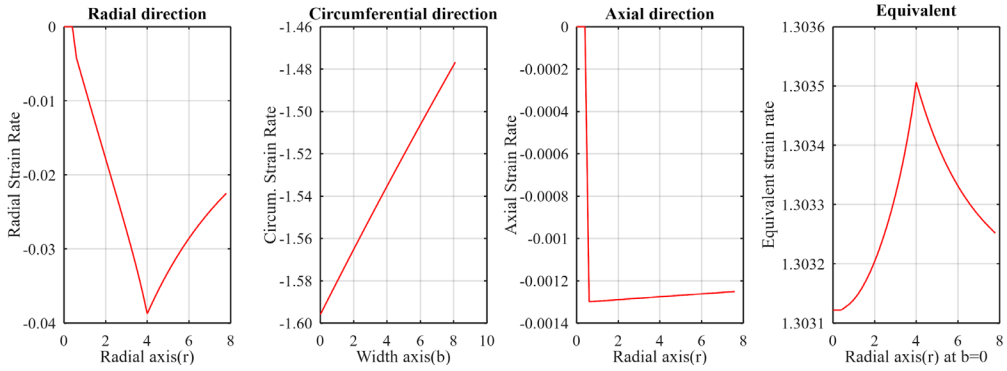

Fig. 6. Radial, circumferential, axial, and von Mises equivalent strain rate distributions for w=25 RPM, f=0.3 mm/s, $t_i = 15$ mm and roller geometry of RG1.

Materials Research Proceedings 28 (2023) 657-666 https://doi.org/10.21741/9781644902479-71

Variations of mean von Mises equivalent strain rate and strain with process parameters are shown in Fig. 7. In each plot, the effect of only one process parameter is tested and other parameters are kept constant. As shown previously, equivalent strain rate distribution is very uniform along the contact zone thus the mean value can represent the deformation behaviour accurately. For strain distribution, however, the mean value provides only a general perspective since strain value increases accumulatively as the circumferential passes form the material.

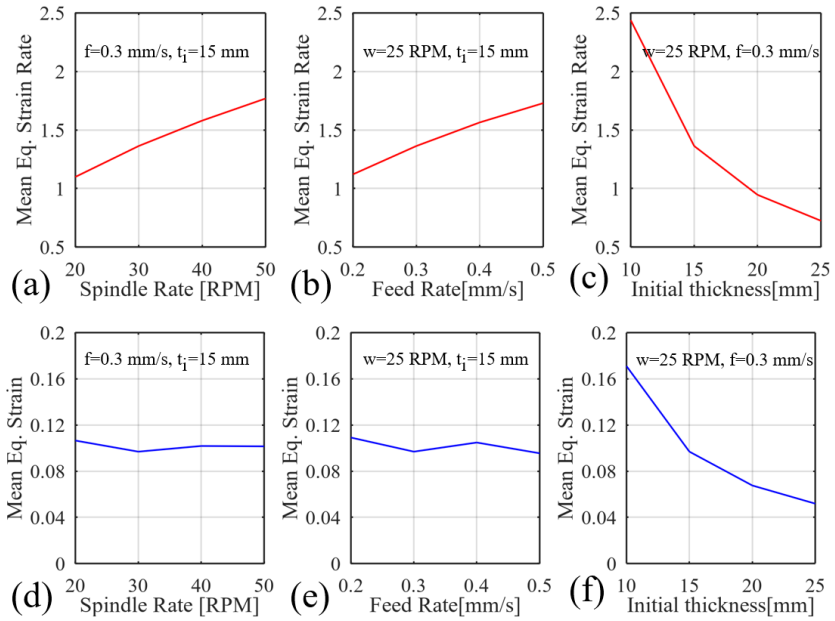

Fig. 7. Mean equivalent strain rate and strain for RG1 roller geometry and varying (a,d) spindle rates, (b,e) feed rates, (c,f) initial thicknesses.

Fig. 7(a) indicates an increase in spindle rate results in a higher mean equivalent strain rate while Fig. 7(d) clearly shows that obtained mean equivalent strains are similar. Positive proportionality between spindle rate and strain rate is due to the higher tangential velocity in the circumferential direction for increasing spindle rate. Even though an increased spindle rate leads to a smaller radial bite which is called pitch, the effect of tangential velocity appears to be higher and overcomes the negative effect of pitch decrease. As the tangential velocity increases, contact time per pass decreases. Consequently, similar mean equivalent strain values are obtained.

A very similar trend is observed for feed rate as shown in Fig. 7(b,e). The equivalent strain rate increases with increasing feed rate but the equivalent strain remains almost constant. As the feed rate is increased while the spindle rate is kept constant, the pitch increases and the tangential velocity does not change. Therefore, a higher equivalent strain rate is obtained for a higher feed rate. Thus the total number of circumferential passes is lower for higher pitch and cumulative strain is similar for different feed rate values. Having similar mean equivalent strain values for different sets of feed rate and spindle rate confirms that the calculated velocity fields are accurate.

Mean strain rate and strain are more sensitive to initial thickness than other parameters as shown in Fig. 7(c,f) For the constant thickness reduction, the proportional decrease in the cross-sectional area during forming is much higher for low initial thicknesses. For different initial thicknesses, the pitch is kept constant and the bite area is not modified. However, the ratio of the bite area to the rest of the circumferential cross-section decreases with increasing initial thickness, and consequently, the strain rate also decreases. For constant feed rate and spindle rate, the total number of passes and contact time per pass do not change. Thus, mean strain rate and strain follow the same trend.

Summary
An analytical method is developed to predict deformation fields for an incremental disk rolling process. Effects of process parameters and roller geometry on the contact zone and plastic deformation fields are examined.

Roller radius is proved to have a considerable effect on the circumferential width of the contact zone which is important for the circumferential plastic deformation. Radial deformation and radial length of the contact zone are mainly controlled by the roller height and the attack angle. Also, nose radius has an important effect on the radial plastic flow since the highest radial strain rate is calculated at the nose-inclined region interface.

The equivalent strain rate is proved to increase with increasing spindle rate due to the higher tangential velocity despite the shorter pitch. It shows that the tangential velocity is more influential on the deformation than the pitch. It can be said that the deformation can be controlled by adjusting the spindle rate without having to modify process time as the process time is controlled by only the feed rate. Increasing the feed rate also causes a higher strain rate but the underlying cause is the higher pitch which enables shorter process time. Therefore a compromise can be established between strain rate and process time by optimizing the process parameters provided that their effects are well understood as aimed by the current study. Strain rate affects recrystallization, failures, forces and related machine requirements as the process time affects grain growth, tool life and related machine requirements. This analytic method plays a key role in machine development as it provides insight into the connection between machine design, process parameters and induced deformation.

Acknowledgement
This work was supported by The Scientific and Technological Research Council of Türkiye, TÜBİTAK.

References
[1] L. Chevalier, Prediction of defects in metal forming: Application to wire drawing, J. Mater. Process. Technol. 32 (1992) 145-153. https://doi.org/10.1016/0924-0136(92)90171-n
[2] J.J. Lee, G.J. Park, Optimization of the structural and process parameters in the sheet metal forming process, J. Mech. Sci. Technol. 28 (2014) 605-619. https://doi.org/10.1007/s12206-013-1125-4
[3] Y.V.R.K. Prasad, T. Seshacharyulu, Modelling of hot deformation for microstructural control, Int. Mater. Rev. 43 (1998) 243-258. https://doi.org/10.1179/imr.1998.43.6.243
[4] X.-M. Chen, Y. C. Lin, M.-S Chen, H.-B. Li, D.-X. Wen, J.-L. Zhang, M. He, Microstructural evolution of a nickel-based superalloy during hot deformation, Mater. Des. 77 (2015) 41-49. https://doi.org/10.1016/j.matdes.2015.04.004
[5] Z. Wusatowski, Fundamentals of Rolling, Pergamon Press, Oxford, 1969
[6] S. Alexandrov, E. Lyamina, Y.R. Jeng, A general kinematically admissible velocity field for axisymmetric forging and its application to hollow disk forging, Int. J. Adv. Manuf. Technol. 88 (2017) 3113-3122. https://doi.org/10.1007/s00170-016-9018-1
[7] J. Zhang, Z. Cui, Prediction of velocity and deformation fields during multipass plate hot rolling by novel mixed analytical-numerical method, J. Iron Steel Res. Int. 18 (2011) 20-27.
[8] S. Serajzadeh, Y. Mahmoodkhani, A combined upper bound and finite element model for prediction of velocity and temperature fields during hot rolling process, Int. J. Mech. Sci. 50 (2008) 1423-1431. https://doi.org/10.1016/j.ijmecsci.2008.07.004
[9] S. Li, Z. Wang, Y. Guo, A novel analytical model for prediction of rolling force in hot strip rolling based on tangent velocity field and MY criterion, J. Manuf. Process. 47 (2019) 202-210. https://doi.org/10.1016/j.jmapro.2019.09.037.

[10] D.H. Zhang, Y.M. Liu, J. Sun, D.W. Zhao, A novel analytical approach to predict rolling force in hot strip finish rolling based on cosine velocity field and equal area criterion, Int. J. Adv. Manuf. Technol. 84 (2016) 843-850. https://doi.org/10.1007/s00170-015-7692-z
[11] S.P. Hamidpour, A. Parvizi, A.S. Nosrati, Upper bound analysis of wire flat rolling with experimental and FEM verifications, Meccanica 54 (2019) 2247-2261. https://doi.org/10.1007/s11012-019-01066-4
[12] H.L. Nascimento, Y. Shigak, S.C. Santos, A.Z. Hubinger, A study of the rolling load calculation models for flat cold rolling process, J. Comput. Meth. Eng. 2 (2016) 320-334.
[13] C.T. Chen, F.F. Ling, Upper-bound solutions to axisymmetric extrusion problems, Int. J. Mech. Sci. 10 (1968) 863-879. https://doi.org/10.1016/0020-7403(68)90090-8
[14] P. Agrawal, S. Aggarwal, N.Banthia, U.S. Singh, A. Kalia, A. Pesin, A comprehensive review on incremental deformation in rolling processes, J. Eng. Appl. Sci. 69 (2022). https://doi.org/10.1186/s44147-022-00072-w
[15] D. Marini, D. Cunningham, J. Corney, A Review of Flow Forming Processes and Mechanisms, Key Eng. Mater. 651-653 (2015) 750-758. https://doi.org/10.4028/www.scientific.net/kem.651-653.750
[16] A. Abedini, S. Rash-Ahmadi, A. Doniavi, Roughness optimization of flow-formed tubes using the Taguchi method, Int. J. Adv. Manuf. Technol. 72 (2014) 1009-1019. https://doi.org/10.1007/s00170-014-5732-8.
[17] S. Fortune, Voronoi Diagrams and Delaunay Triangulations, in: D.Z. Du, F. Hwang (Eds.), Computing in Euclidean Geometry, 1995, pp. 225-265.